Characterisation of dynamic behaviour of alumina ceramics: evaluation of stress uniformity

Zhiyong Wang and , and Peifeng Li

Citation: AIP Advances **5**, 107224 (2015); doi: 10.1063/1.4934793
View online: http://dx.doi.org/10.1063/1.4934793
View Table of Contents: http://aip.scitation.org/toc/adv/5/10
Published by the American Institute of Physics

Characterisation of dynamic behaviour of alumina ceramics: evaluation of stress uniformity

Zhiyong Wang and Peifeng Li[a]
School of Mechanical and Aerospace Engineering, Nanyang Technological University, Singapore

(Received 7 August 2015; accepted 13 October 2015; published online 23 October 2015)

Accurate characterisation of dynamic behaviour of ceramics requires the reliable split-Hopkinson pressure bar (SHPB) technique and the condition of uniaxial homogeneous specimen deformation. In this study, an experimentally validated 3D finite element model of the full scale SHPB experiment was developed to quantitatively evaluate the wave propagation in the bars and the stress distribution/evolution in the alumina specimen. Wave signals in both the SHPB experiments and the finite element model were analysed to characterise the dynamic behaviour of alumina. It was found that the equilibrium of both stresses within the specimen and forces at the specimen ends can be established in the intermediate stage of deformation. The validity of stress uniformity in the alumina specimen supports the assumption of uniaxial homogeneous specimen deformation in the SHPB and validates the characterisation of dynamic behaviour of alumina ceramics. [http://dx.doi.org/10.1063/1.4934793]

I. INTRODUCTION

Ceramic materials are increasingly used in armour applications due to their light weight and high compressive strength. The dynamic behaviour of these materials needs to be accurately characterised in order to predict their service performance.[1–8] The high rate properties of ceramics can be typically measured using the split-Hopkinson pressure (SHPB) technique.[2,5,6,8] Initially developed to measure the dynamic behaviour of metals,[9–12] the SHPB technique has been modified to test other materials such as polymer and foams.[13,14] However, to accurately characterise the behaviour of ceramics at high strain rates on the order of 10^3 s^{-1} using the SHPB is still a challenge as a result of the high failure strength and the low failure strain (typically less than 2%).[7,15–17] This requires not only the modification of the SHPB experimental technique and the specimen design but also the valid test conditions such as the stress uniformity in the specimen.

Stress and strain histories in a specimen can be calculated using the force and velocity at the two bar-specimen interfaces on the assumption of one-dimensional wave propagation theory and uniaxial homogeneous deformation of specimens. However, strain gauges are usually mounted away from the bar-specimen interface in the SHPB system, e.g., in the middle of the bars, in order to avoid the superposition of wave signals near the interface. Even though the wave signals can be aligned to the bar-specimen interfaces, few studies[18,19] examined the stress equilibrium in specimens, the condition for a valid SHPB test. It was reported that the inertial and wave propagation can affect the stress differences between the ends of compression SHPB specimens.[18] However, the experimental and analytical approach can be used to examine the force equilibrium between specimen ends but not the stress state within the specimen.

Numerical simulation such as finite element (FE) model has been used to investigate the stress evolution in materials subjected to dynamic impact loads.[15,20–22] Although FE modelling has been applied to simulate the wave propagation in an SHPB test of ceramics,[21] most of the previous FE

[a]Corresponding author's email: peifeng.li@ntu.edu.sg (P. Li); Tel: +65 6790 4766.

models for ceramics focused on the evolution of damage during the impact process.[15,20,22] Numerical simulation provides an effective way to examine the forces at the bar-specimen interfaces and the stress distribution in the ceramics, and thus to verify the uniaxial homogeneous deformation of the specimen during the SHPB process.

The aim of this study was to investigate the stress uniformity in the SHPB test of alumina ceramics for the reliable characterisation of the dynamic response. A 3D FE model consisting of the full scale SPHB bars and the ceramic specimen was developed to predict the wave propagation in the bars and the stress distribution/evolution in the specimen. The stress uniformity within the specimen as well as the force equilibrium at the interfaces was analysed and evaluated to validate the condition of the SHPB test and allow for the accurate characterisation of dynamic behaviour of alumina.

II. SPLIT-HOPKINSON PRESSURE BAR EXPERIMENTS

Uniaxial dynamic compression experiments of alumina ceramics were conducted in an in-house split-Hopkinson pressure bar system (Fig. 1(a)). The SHPB system consisted of D_0 = 20 mm diameter striker, input and output bars with the length of 400 mm, 1200 mm and 1200 mm, respectively. The bars were all made of YAG300 maraging steel (Young's modulus E_0 = 184 GPa, Poisson's ratio ν_0 = 0.30, density ρ_0 = 8030 kg m^{-3}, and thus wave velocity $c_0 = \sqrt{E_0/\rho_0}$ = 4786 m s^{-1}).

Cylindrical alumina specimens (Chair Man Hi-Tech Co. Ltd., Taiwan) of the diameter D = 5 mm and length l = 5 mm were prepared and placed between the input and output bars during

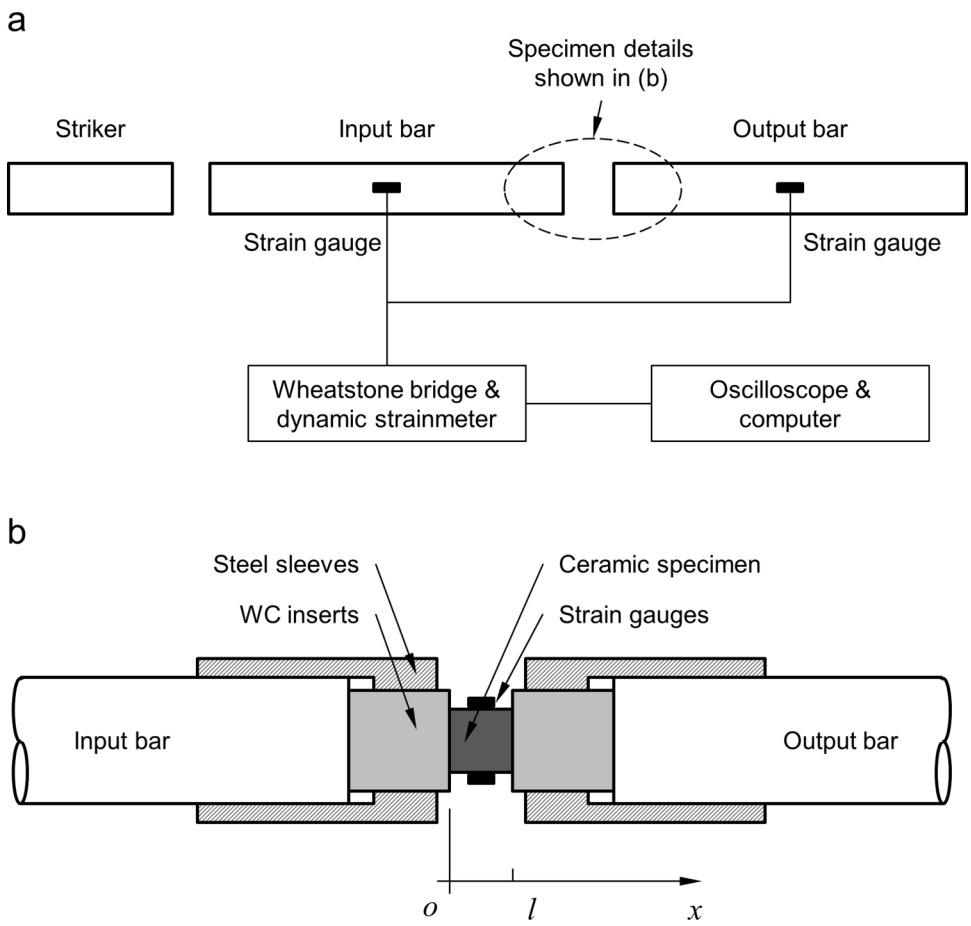

FIG. 1. The split-Hopkinson pressure bar (SHPB) system: (a) the schematic of SHPB configuration, and (b) the setup of ceramic specimen and the definition of one-dimensional coordinate system.

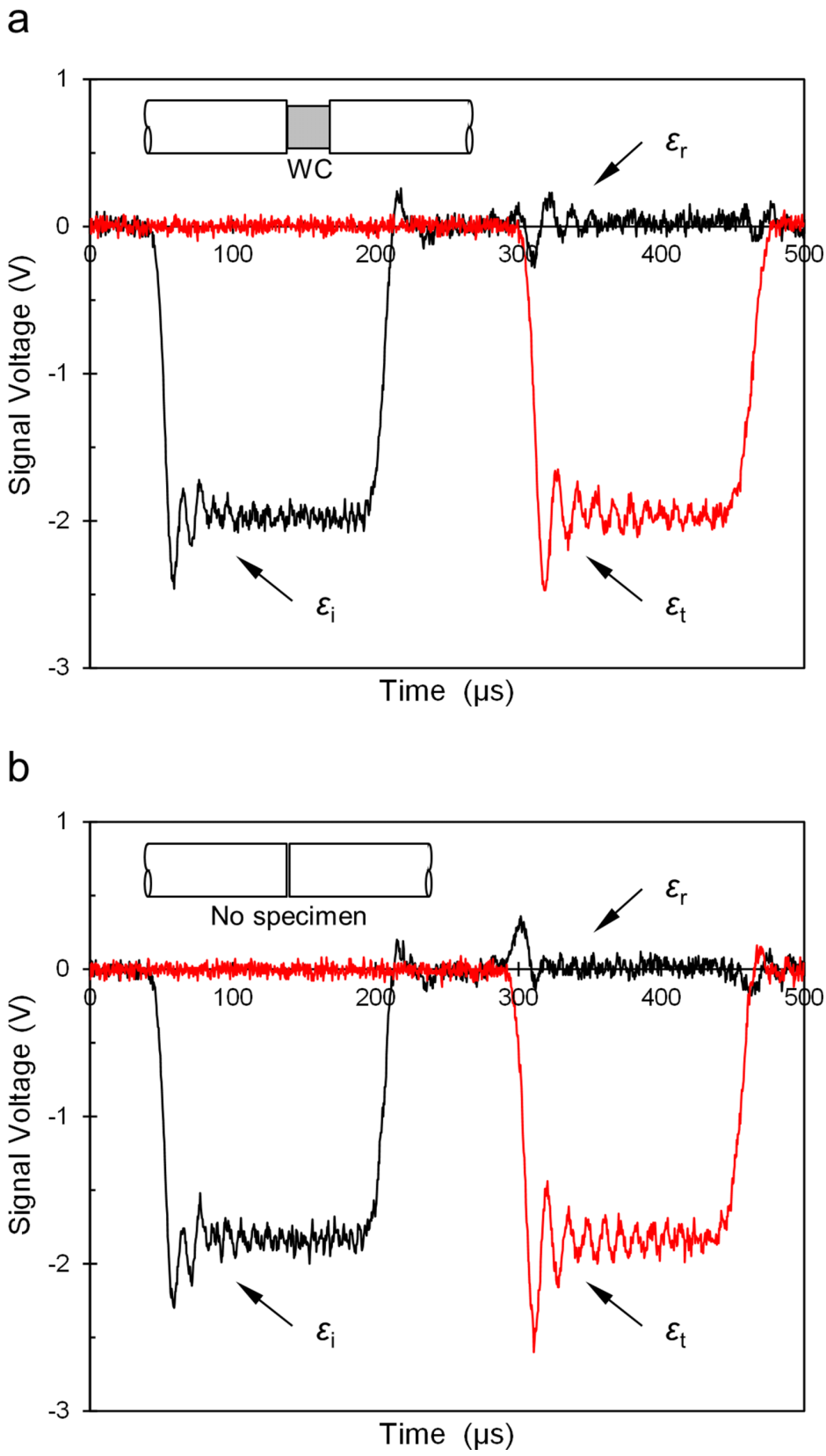

FIG. 2. Recorded wave signals in two SHPB tests to verify the impedance match between the WC inserts and bars: (a) a WC insert as the specimen, and (b) no specimen.

the SHPB experiments. In an SHPB test, the impact by the striker with an initial velocity ~20 m s^{-1} generates an elastic pulse (called incident wave, σ_i or ε_i in terms of bar stress or strain, respectively) in the input bar that propagates towards the specimen. When the incident wave reaches the bar-specimen interface, a portion of the wave (reflected wave, σ_r or ε_r) is reflected back into the input bar, and the remaining portion (transmitted wave, σ_t or ε_t) is transmitted into the output bar through the specimen. Strain gauges were mounted approximately in the middle of the bars to record these waves through the Wheatstone half bridge circuits, TML (Tokyo Sokki Kenkyujo Co. Ltd., Japan) dynamic strainmeter and Yokogawa (Yokogawa Electric Corp., Japan) oscilloscope (Fig. 1(a)).

To avoid the indentation into the steel bars caused by the harder ceramic specimens, a pair of cylindrical tungsten carbide (WC, diameter D_{WC} = 17 mm and length l_{WC} = 17 mm, Young's modulus E_{WC} = 546 GPa, density ρ_{WC} = 15000 kg m^{-3}, and thus wave velocity $c_{WC} = \sqrt{E_{WC}/\rho_{WC}}$ = 6033 m s^{-1}) inserts was sandwiched between the bars and the specimen (see Fig. 1(b)).[2,23] The theoretical diameter of the WC inserts is approximately 13 mm in order to achieve the match of the general wave impedance between the WC inserts and the maraging steel bars (i.e. $\rho_{WC}c_{WC}A_{WC} = \rho_0 c_0 A_0$). However, considering the imperfect interface, a larger diameter (17 mm) was actually used for the WC inserts. In the SHPB test on a WC insert being the specimen, the entire incident wave was transmitted with negligible losses and was not reflected at the bar-insert interface (Fig. 2(a)); this is similar to the wave propagation in the dummy test without a specimen (Fig. 2(b)). Therefore, the agreement supports the design of the actual diameter D_{WC} = 17 mm of the WC inserts. The steel sleeves were used to confine and further strengthen the WC inserts such that the ceramic specimen failed before the inserts did (Fig. 1(b)).

A pair of strain gauges, forming part of a Wheatstone half bridge circuit, was mounted on the opposite surfaces of specimens (Fig. 1(b)) to directly measure the strain history in the specimen. It is often difficult to measure the entire strain history as a result of the earlier failure of strain gauges caused by crack propagation in the specimen. However, the strain history, incompletely but directly measured, can be used to validate the calculated strain as will be discussed below.

III. FINITE ELEMENT MODELLING

A 3D FE model using the ABAQUS/Explicit solver (Dassault Systèmes Simulia Corp., RI, USA) was developed to simulate the strain wave propagation in the bars and the stress distribution/evolution in the alumina during an SHPB experiment. The FE model consisted of the full scale geometries of the striker, input and output bars as well as the WC inserts and alumina specimen (Fig. 3). Hexahedral elements were used to mesh the FE model. The mesh density in the SHPB system was investigated in terms of both the computational efficiency and accuracy. The radii of the alumina, WC inserts and SHPB bars were then meshed with 25, 20 and 10 FE elements, respectively (see Fig. 3). Details on the geometrical model can be found in the work.[15]

An initial impact velocity of 20 m s^{-1} was applied to the striker. A frictional coefficient of 0.06 was defined for all the interfacial contacts in the SHPB system, e.g., the interface between the striker and input bar. The elastic material data were specified for the striker, input and output bars and the WC inserts.

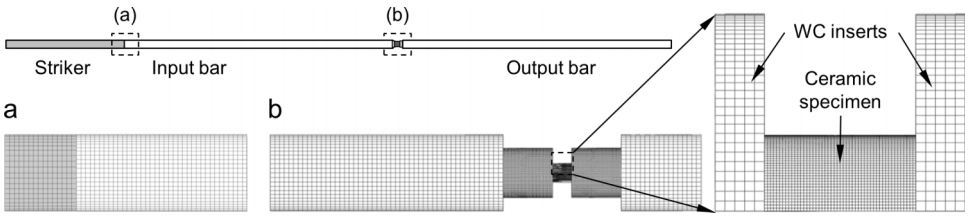

FIG. 3. The full scale geometrical model of an SHPB test of a ceramic specimen and the varied FE meshes in the specimen, SHPB bars and WC inserts.

TABLE I. Constitutive parameters for the JH-2 model of alumina.

Parameter	Value
Density (kg m^{-3}), ρ	3860
Young's modulus (GPa), E	390
Shear modulus (GPa), G	157
Intact strength coefficient, A	0.958
Intact strength exponent, N	0.243
Fracture strength coefficient, B	0.45[a]
Fracture strength exponent, M	0.6[a]
Strain rate coefficient, C	0.0076
Hydro tensile limit (MPa), T	462[a]
Hugoniot elastic limit (MPa), HEL	7000[a]
Bulk modulus (GPa), K_1	250
Pressure coefficient (GPa), K_2	-274
Pressure coefficient (GPa), K_3	2934
Damage coefficient, D_1	0.1
Damage coefficient, D_2	0.7

[a]Note: data were obtained from the literature.[20]

The constitutive behaviour of alumina ceramics at high strain rates was quantified using the Johnson-Holmquist material model with damage (JH-2), a widely accepted model for brittle materials subjected to high loading rates, high pressure and large deformation.[24] To describe the mechanical behaviour of ceramics, the JH-2 model considers the equation of state (EOS) in a polynomial form, the specific strength model for both the intact and fractured materials and the damage evolution rule. The polynomial EOS evaluates the current pressure state by the variation of volumetric strains. The damage model determines the occurrence of fracture in ceramics. Most of the constitutive parameters for the JH-2 model of alumina (Table I) were obtained from the SHPB experiment in this study; only a few parameters were from the literature.[20]

The stress (σ_i, σ_r and σ_t) or strain (ε_i, ε_r and ε_t) waves in the bars, measured during the SPHB tests and predicted in the FE model, were analysed to reduce noises by filtering the high frequency oscillation, correct the wave dispersion, and subsequently align to the bar-specimen interfaces (refer to Fig. 4). On the assumption of axial uniformity of specimen stress and strain fields as will be discussed in Sections IV C and IV D:

$$\varepsilon_i + \varepsilon_r = \varepsilon_t \tag{1}$$

the average stress (σ) and strain (ε) history of the specimen can be calculated as follows:

$$\sigma(t) = \frac{A_0 E_0}{A}\varepsilon_t(t) \tag{2}$$

$$\varepsilon(t) = \frac{2c_0}{l}\int_0^t [\varepsilon_i(\tau) - \varepsilon_t(\tau)]\, d\tau \tag{3}$$

where A_0 ($= \pi {D_0}^2/4$) and A ($= \pi D^2/4$) are the cross-sectional areas of the bars and the specimen respectively, and t is the time.

IV. RESULTS AND DISCUSSION

A. Analysis of strain waves in SHPB experiments

Fig. 5 illustrates the representative wave signals recorded in an SHPB test of alumina. The noise of wave signals was reduced in the post-test fast Fourier transform (FFT) algorithm by filtering the high frequency (≥100 kHz) oscillation. Fig. 5(b) shows a good agreement between the rising

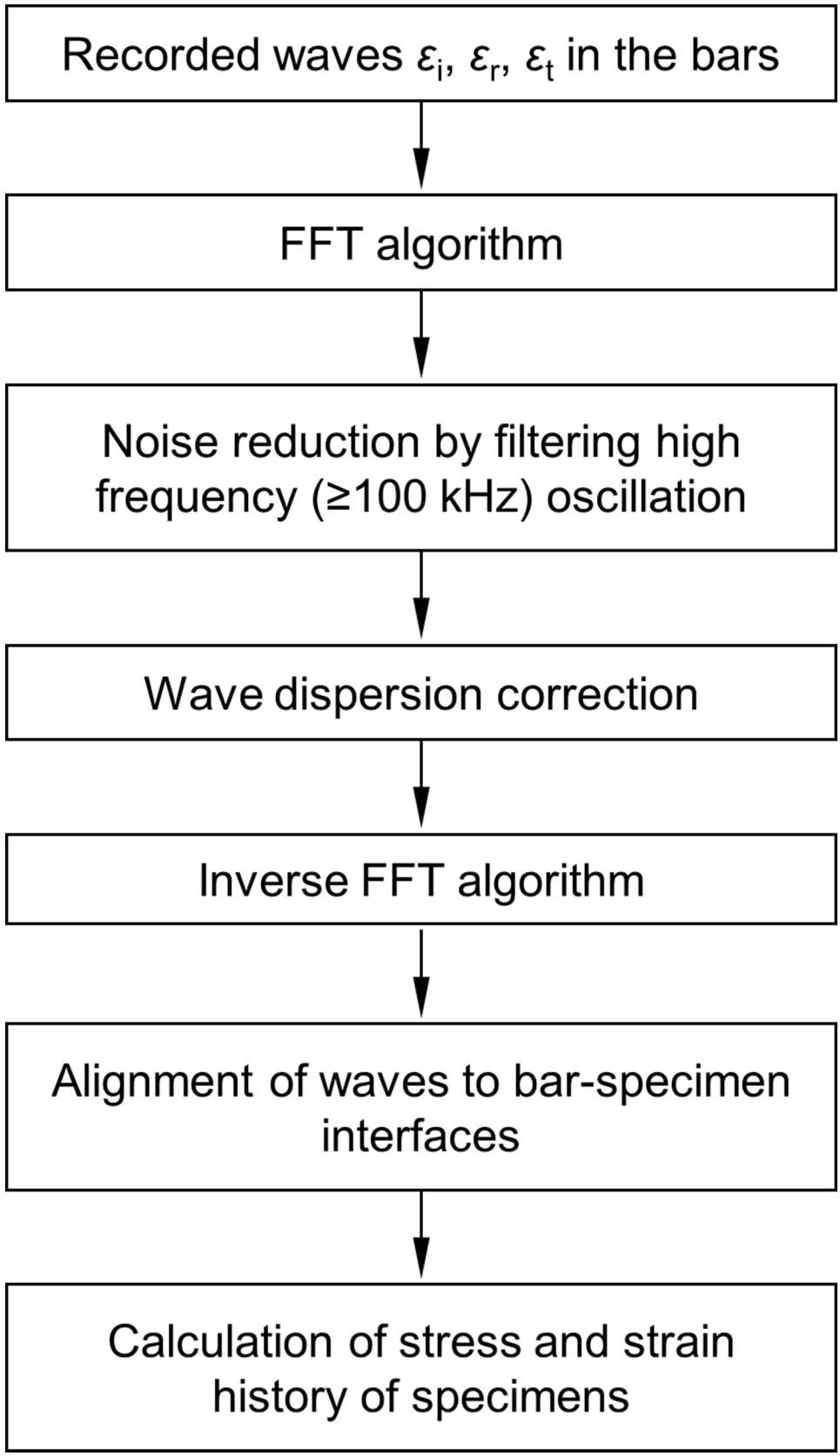

FIG. 4. The procedure to analyse wave signals recorded in SHPB bars to calculate stress and strain histories of specimens.

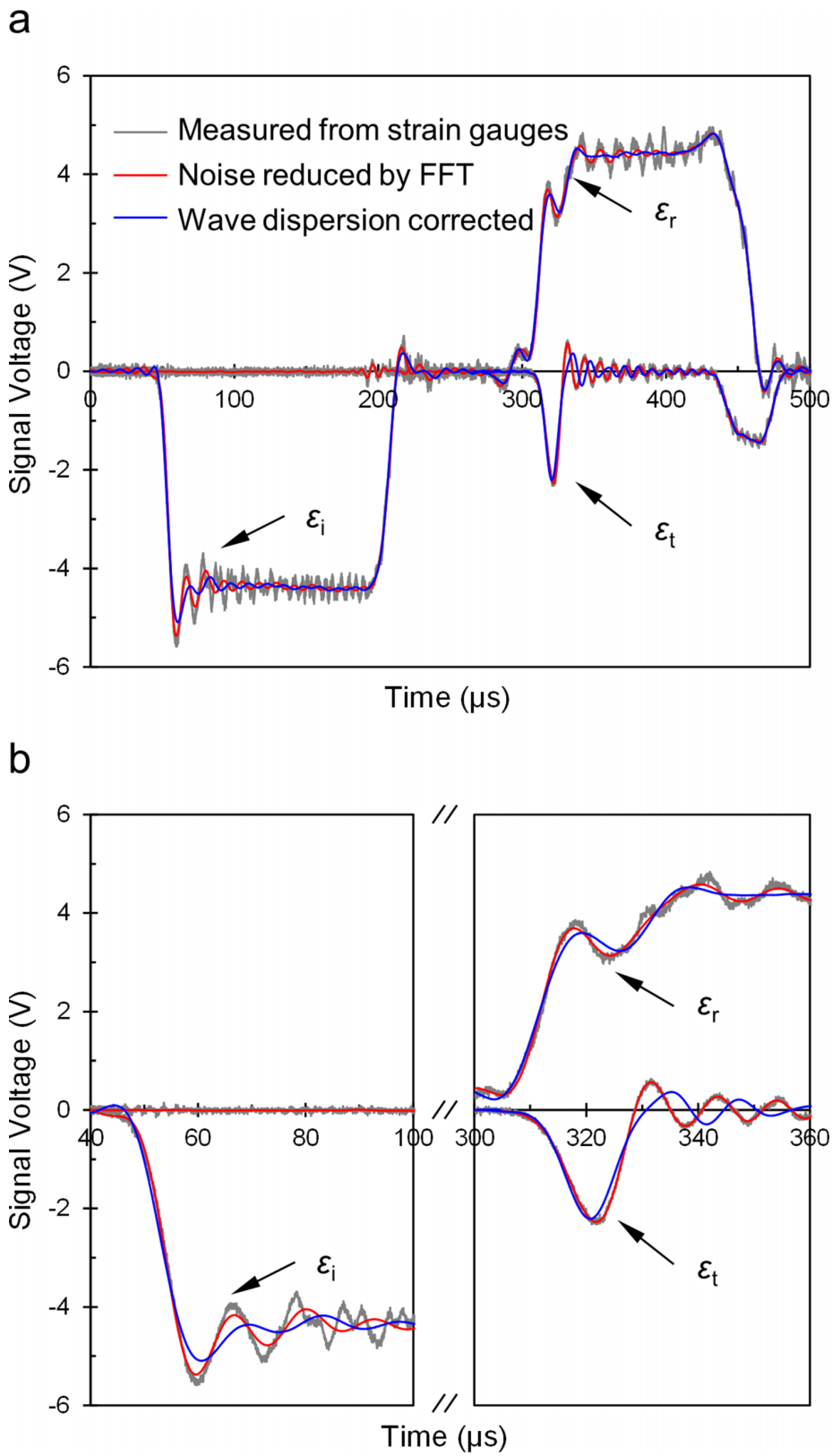

FIG. 5. Noise reduction by filtering high frequency oscillation (red) and subsequent wave dispersion correction (blue) of the recorded wave signals (black) in an SHPB test: (a) a full period, and (b) zoom in views to highlight the signal process in the rising stage of incident, reflected and transmitted waves.

edges of the wave signals before and after filtering the high frequency components by FFT. Correction of the wave dispersion in the frequency domain using an FFT algorithm was conducted to reconstruct strain waves $\varepsilon(x_0+\Delta x, t)$ at the bar-specimen interfaces $(x_0+\Delta x)$ from the waves $\varepsilon(x_0, t)$ measured in the strain gauge locations (x_0).[25] Note that $\varepsilon(x_0, t)$ can be ε_i, ε_r and ε_t as measured in the strain gauges. Following wave dispersion correction (Fig. 5), the processed signals ε_i and ε_r represented the wave histories at the input bar-specimen interface while ε_t was reconstructed to the output bar-specimen interface.

To accurately synchronise the three corrected strain waves, the imaginary reflected (ε_r) and transmitted (ε_t) waves were predicted for the known incident (ε_i) wave and a fictitious elastic specimen assumed to have a Young's modulus equal to that of the real alumina specimen. A direct Laplace-transform analytical solution of the wave propagation equation in the fictitious specimen was introduced to calculate the imaginary reflected and transmitted waves as follows:

$$\varepsilon_r(t) = \frac{1-r}{1+r}\varepsilon_i(t)u(t) - \frac{4r}{1-r}\sum_{k=1}^{\infty}\frac{(1-r)^{2k}}{(1+r)^{2k+1}}\varepsilon_i(t-2k\tau)u(t-2k\tau) \tag{4}$$

$$\varepsilon_t(t) = \frac{4r}{(1+r)^2}\varepsilon_i(t-\tau)u(t-\tau) + \frac{4r}{1+r}\sum_{k=1}^{\infty}\frac{(1-r)^{2k}}{(1+r)^{2k+1}}\varepsilon_i(t-(2k+1)\tau)u(t-(2k+1)\tau) \tag{5}$$

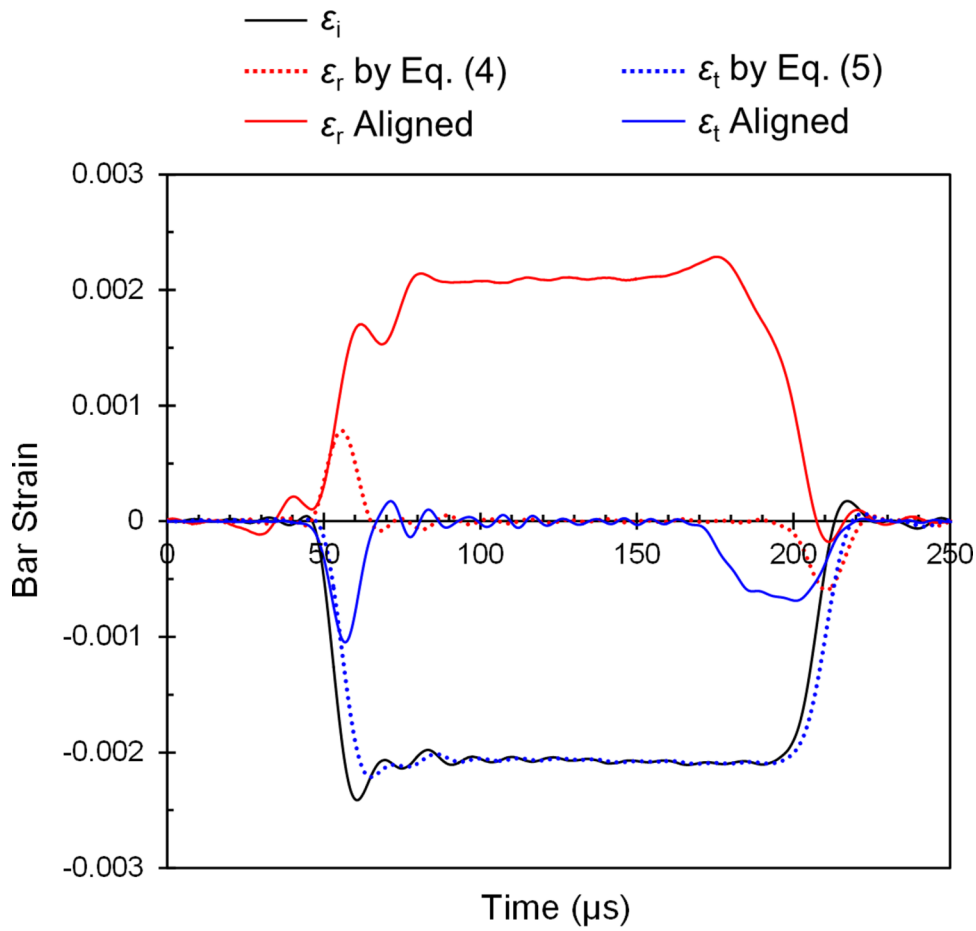

FIG. 6. Alignment of reflected and transmitted strain waves to the incident wave in SHPB testing. Both reflected and transmitted waves were shifted based on the shapes of corresponding waves (dotted lines) that were predicted by Eqs. (4) and (5).

where $r = (\rho_0 c_0 A_0)/(\rho c A)$ is the generalised wave impedance ratio between the bars and specimen (density ρ and wave velocity c for the specimen), $u(t)$ is the unit step function, and $\tau = l/c$ is the wave travel time between the specimen ends (equal to half a propagation cycle 2τ). Fig. 6 shows the two fictitious reflected and transmitted waves as predicted using Eqs. (4) and (5). The predicted profiles are similar to the actual waves as measured in the SHPB test of real alumina only in the early stage (initial part of the rising edge), because the wave propagation in the specimen is assumed to be totally elastic in the test.

Fig. 6 also illustrates that the measured reflected and transmitted waves, following wave dispersion correction, were shifted to synchronise the incident wave so that their rising edges matched those of the corresponding predicted fictitious waves. In the SHPB experiment, ceramic specimens start to deform elastically in the early stage (represented by the rising edge of waves), although inelastic deformation can arise under further loading.[2,15] The alignment of the waves was then justified because comparison of the wave shapes was only made in the rising edges of the waves. Therefore the three synchronised ε_i, ε_r and ε_t represented the strain waves at the bar-specimen interfaces (Fig. 6).

B. Validation of strain wave predictions

With an initial striker velocity of 20 m s^{-1}, the propagation of elastic strain waves in the bars was simulated in the FE model of the full scale SHPB system. The predicted strain waves (ε_i, ε_r and ε_t) in the middle of the input and output bars were compared to the waves that were measured during the SPHB experiments (Fig. 7). Note that the experimentally measured strain waves shown in Fig. 7 were processed to reduce noise that arose due to the recording equipment; but such noise is not expected in the FE model. For the comparison purpose, the time was synchronised to that in the

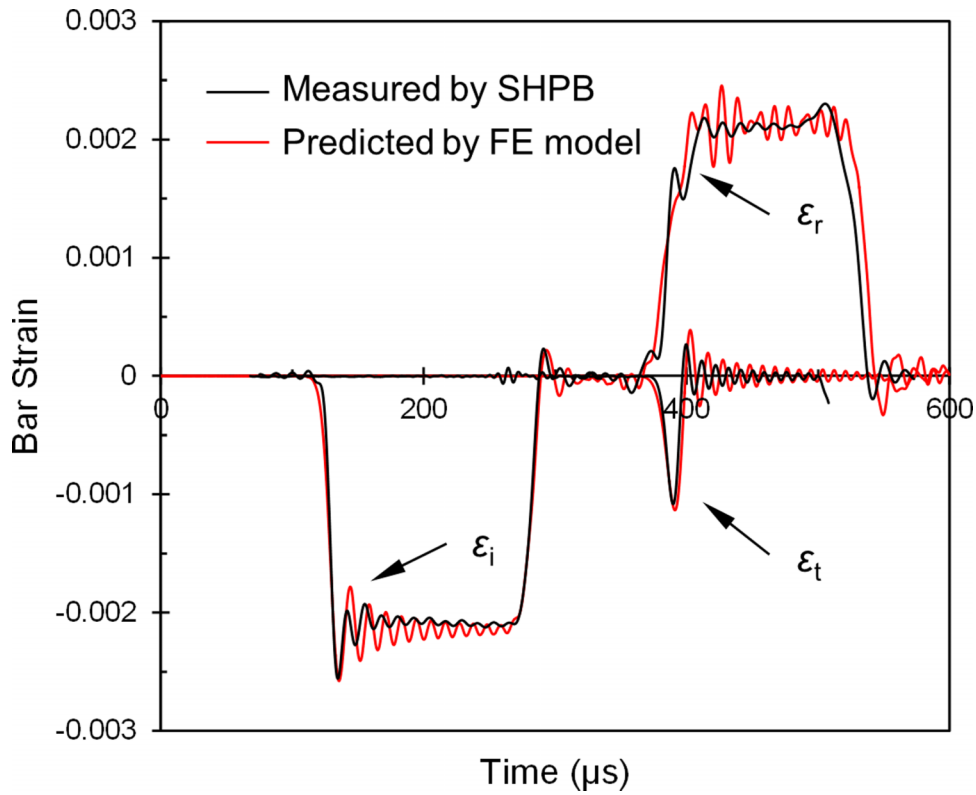

FIG. 7. Comparison of strain waves in the SHPB system: experimental measurement versus FE prediction. (Note: the noise was analytically filtered in the experimental results.)

model. The agreement between the experimental and simulated strain waves (Fig. 7) validates the FE model of SHPB compression as well as the use of JH-2 material model for alumina.

The analysis method as demonstrated in Fig. 4 was also applied to process the strain waves in the middle of the input and output bars predicted in the FE model, including correction of wave dispersion and alignment to the bar-specimen interfaces. Similarly, using Eqs. (4) and (5), the fictitious reflected and transmitted strain waves at the bar-specimen interfaces were calculated in an SHPB test of a fully elastic ceramic. As shown in Fig. 8, these two fictitious waves are consistent with the strain waves at the bar-specimen interfaces that were directly predicted by the full scale SHPB FE model on the fully elastic alumina (without considering the inelastic behaviour). The consistency further supports the developed FE model and the material constitutive formulation.

C. Force equilibrium

To verify the assumption of axial deformation uniformity in a specimen as defined by Eq. (1) such that the specimen stress and strain histories can be calculated, this study also examined the equilibrium of forces at the input (F_{in}) and output (F_{out}) ends of a specimen. The forces can be calculated in terms of the known ε_i, ε_r and ε_t strain waves at the bar-specimen interfaces:

$$F_{in}(t) = E_0 A_0 [\varepsilon_i(t) + \varepsilon_r(t)] \tag{6}$$

$$F_{out}(t) = E_0 A_0 \varepsilon_t(t) \tag{7}$$

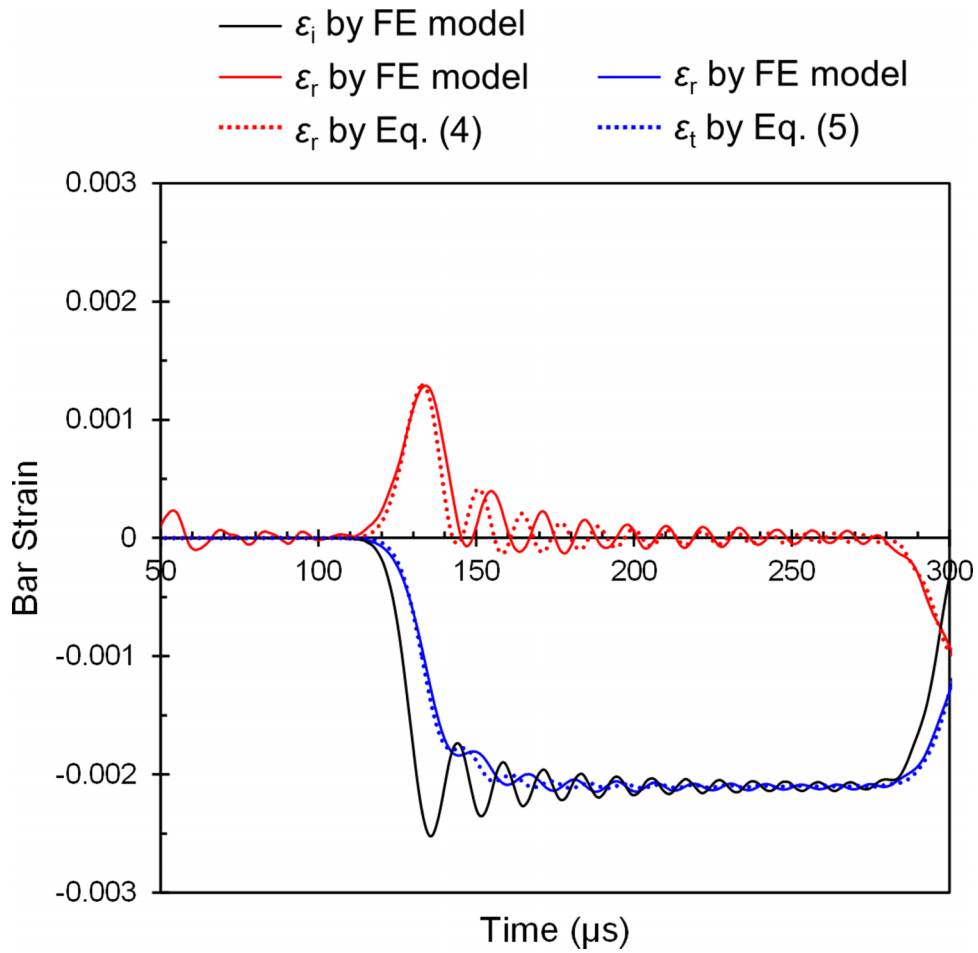

FIG. 8. Comparison of reflected and transmitted strain waves in an SHPB test of a fully elastic ceramic: FE prediction versus analytical calculation using Eqs. (4) and (5).

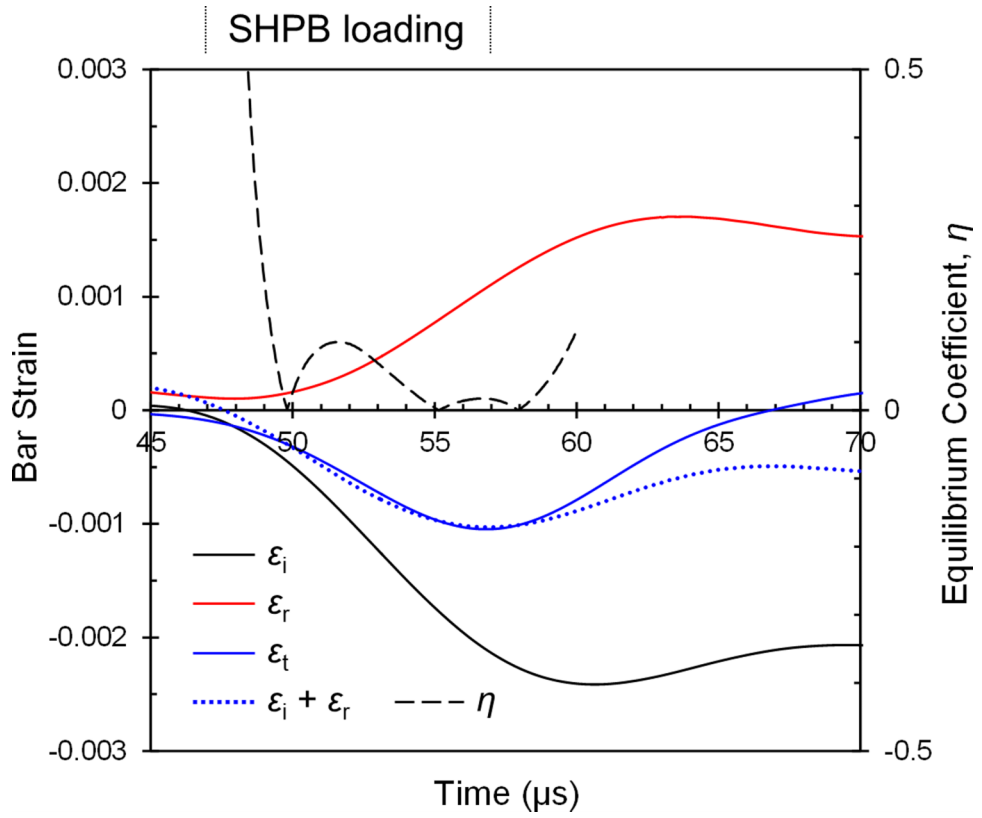

FIG. 9. Verification of force equilibrium at specimen ends in the SHPB experiment of alumina specimens. Transmitted strain wave was compared to the sum of incident and reflected strain waves. Force equilibrium was further quantified by the coefficient η.

To quantify the force equilibrium, a coefficient (η) was defined by normalising the difference between the forces at the specimen ends with their average ($(F_{in} + F_{out})/2$):[21]

$$\eta = 2\left|\frac{F_{in} - F_{out}}{F_{in} + F_{out}}\right| = 2\left|\frac{\varepsilon_i + \varepsilon_r - \varepsilon_t}{\varepsilon_i + \varepsilon_r + \varepsilon_t}\right| \tag{8}$$

Figs. 9 and 10 illustrate the evolution of equilibrium coefficient η during the SHPB compression of alumina, which was calculated based on the strain waves obtained from the experiment and the FE prediction, respectively. The forces are not in equilibrium at the very early stage of SHPB compression of alumina. The coefficient η reduces to <5% after ~5 μs that is equivalent to ~5 wave travel cycles within the specimens. Note that a wave propagation cycle $2\tau = 2l/c \approx 1.0$ μs for alumina. The stress can be considered to be equilibrated if the η is less than 5%.[16,21] Therefore, the force equilibrium at the two ends of the specimen is established in the intermediate stage of deformation during the SHPB compression.

D. Stress uniformity

The predicted stress distribution and its evolution with time (refer to Fig. 11) were examined to verify the equilibrium of stress within the alumina during the SHPB compression. At the early stage of SHPB loading (e.g. at 121 μs in the FE model, refer to Fig. 11(a)), the stresses are non-uniformly distributed throughout the alumina, especially at the ends due to the interfacial friction. However, a more uniform stress field can be observed at the intermedidate stage of the loading (e.g., at 130 μs in Fig. 11(b)).

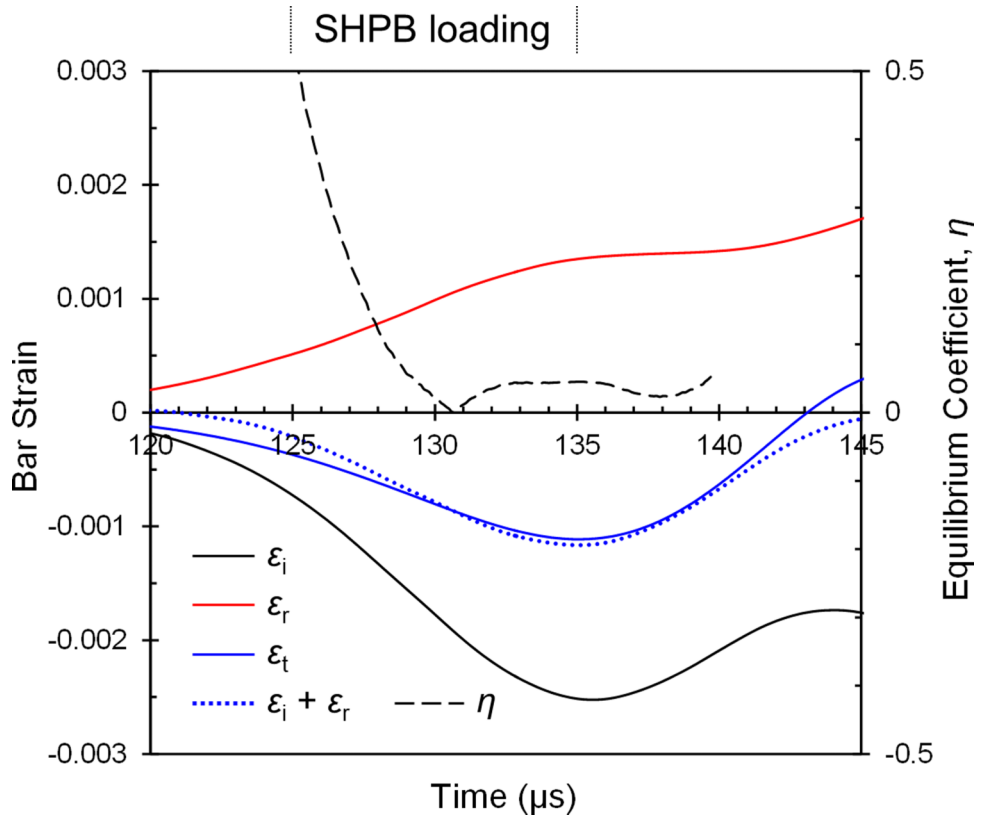

FIG. 10. FE prediction of force equilibrium at specimen ends in the SHPB compression of alumina. Transmitted strain wave was compared to the sum of incident and reflected strain waves. Force equilibrium was further quantified by the coefficient η.

The coefficient of variation (C_v), defined as the ratio of the standard deviation (S_σ) to the average ($\bar{\sigma}$) of stresses, was used to quantify the stress equilibrium in the alumina specimen:

$$C_v = \left| \frac{S_\sigma}{\bar{\sigma}} \right| \tag{9}$$

The C_v was calculated based on the predicted stress distribution in the entire volume ($C_{v,\,vol}$) and along the central line ($C_{v,\,line}$) in the specimen (see Fig. 12). The $C_{v,\,vol}$ is approximately ten times greater because the significant stress concentration occurs in the specimen especially at the corners. However, as the SHPB load is applied, both the $C_{v,\,vol}$ and $C_{v,\,line}$ gradually decrease and become convergent to 0.17 and 0.02, respectively, after ~5 μs of SHPB loading. The convergence of both $C_{v,\,vol}$ and $C_{v,\,line}$ implies a possible equilibrium of stress in the alumina specimen in the intermediate stage of deformation. Therefore, the assumption of axial uniformity of specimen stress and strain field as defined by Eq. (1) is validated in the SHPB test of alumina.

E. Quantification of dynamic behaviour of alumina

The stress and strain history of the specimens was calculated from the aligned ε_i, ε_r and ε_t waves using Eqs. (2) and (3) (see Fig. 13). The specimen strain was also measured directly from the strain gauges mounted on the specimen surfaces. But only the initial portion of strain history was recorded because crack propagation on specimen surfaces induces the early failure of strain gauges prior to the facture of ceramic specimens. The good agreement between the calculated and measured strains in specimens thus supports the alignment of strain waves and the use of two-wave analysis (Eq. (3)) to calculate the strain. The calculation of specimen strains based on the measured

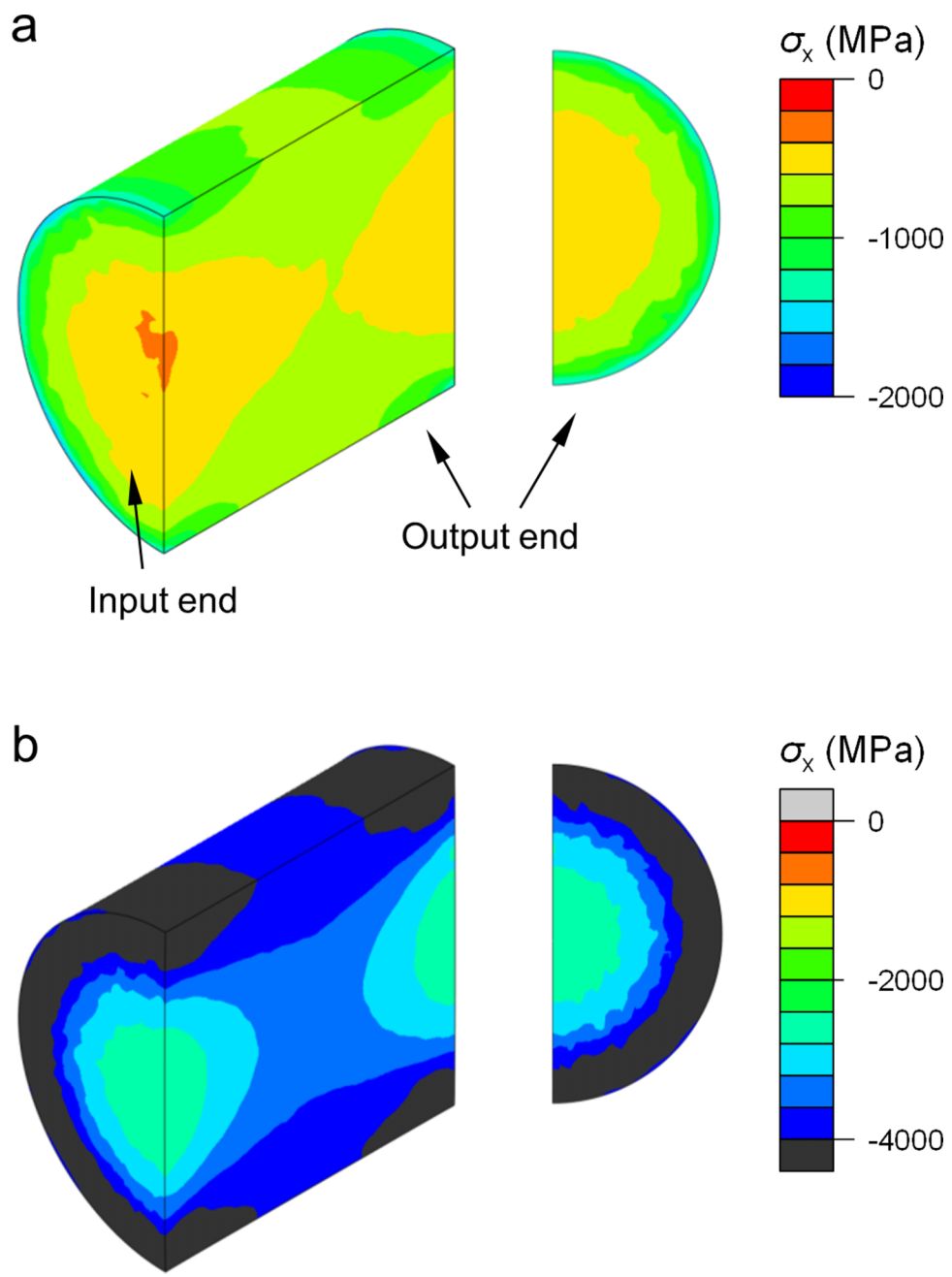

FIG. 11. Predicted longitudinal axial stress distribution within an alumina specimen at the two stages of an SHPB compression: (a) 121 μs and (b) 130 μs (refer to the time scale in Fig. 10).

strain waves in the SHPB bars avoids mounting strain gauges on specimens and thus allows for the in-situ observation of failure process in ceramics using high speed photography.[15,26]

The dynamic strain rate can be estimated to be ~2000 s^{-1} using the average slope of the approximately linear portion of strain curves immediately prior to the fracture of alumina specimens (Fig. 13). Fig. 14 illustrates the representative stress versus time curves of alumina measured in the SHPB tests. The dynamic stress versus time curve was also calculated using the strain waves in the middle of the input and output bars as predicted by the full scale FE model (Fig. 14). The stress versus time curve predicted by the FE model agrees well with those measured in the SHPB experiments.

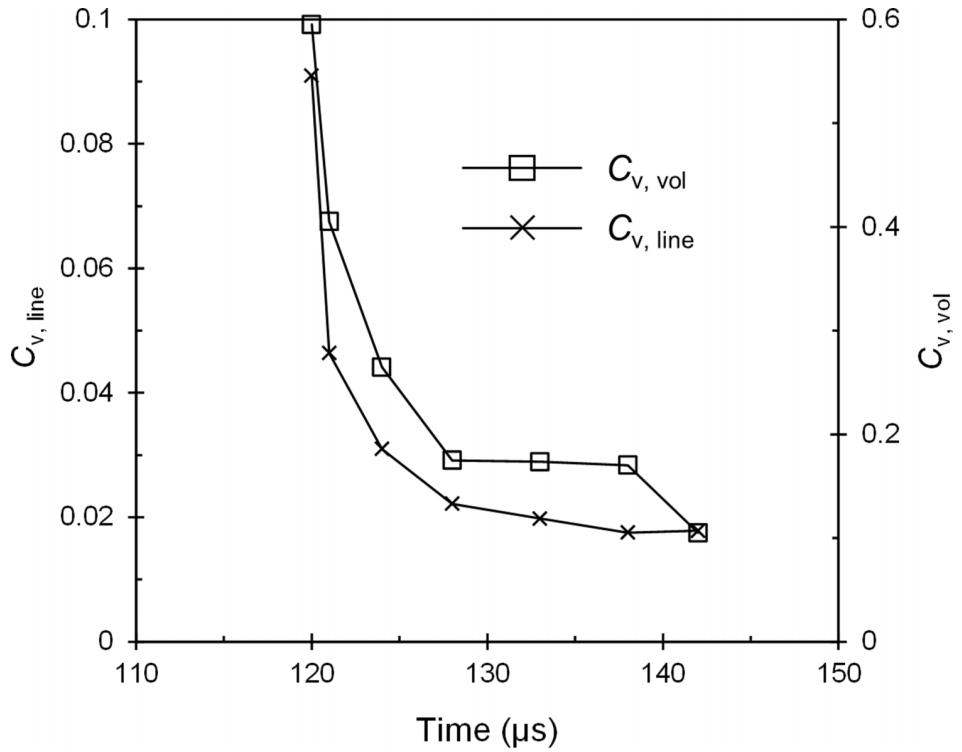

FIG. 12. Verification of specimen stress equilibrium in an SHPB experiment of alumina by the coefficient of variation of stress distribution in the entire volume ($C_{v,\ vol}$) and along the central line ($C_{v,\ line}$).

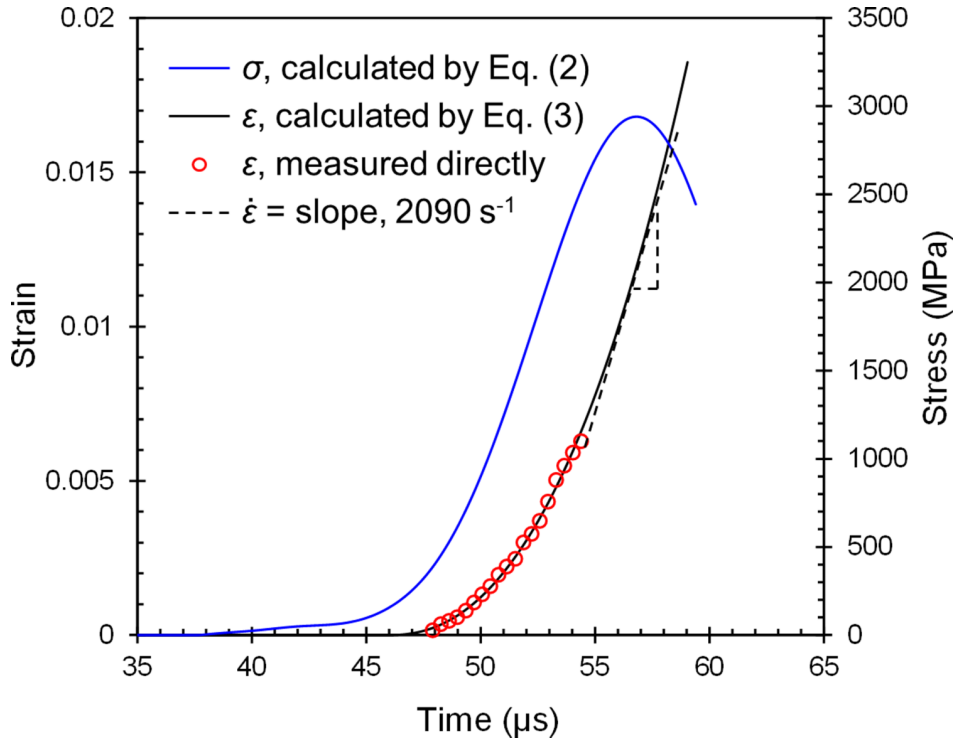

FIG. 13. Stress and strain history of specimens calculated from the bar wave signals in SHPB testing. Calculated strains were compared to those measured directly from strain gauges on alumina specimens.

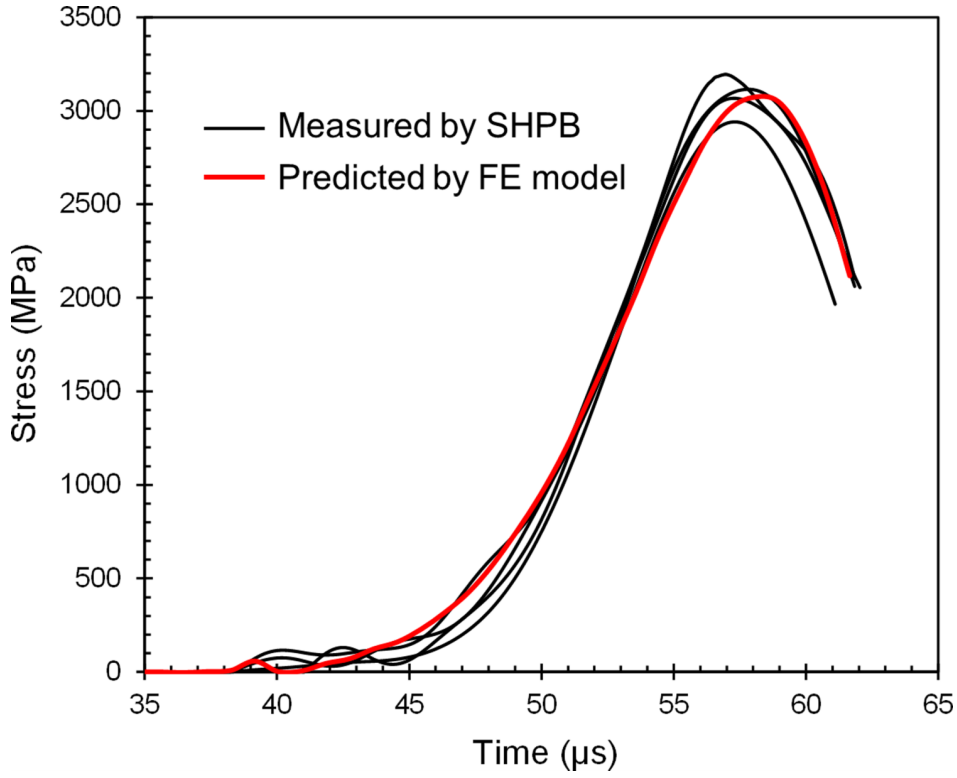

FIG. 14. Comparison between experimentally measured and FE predicted stress versus time curves in the SHPB.

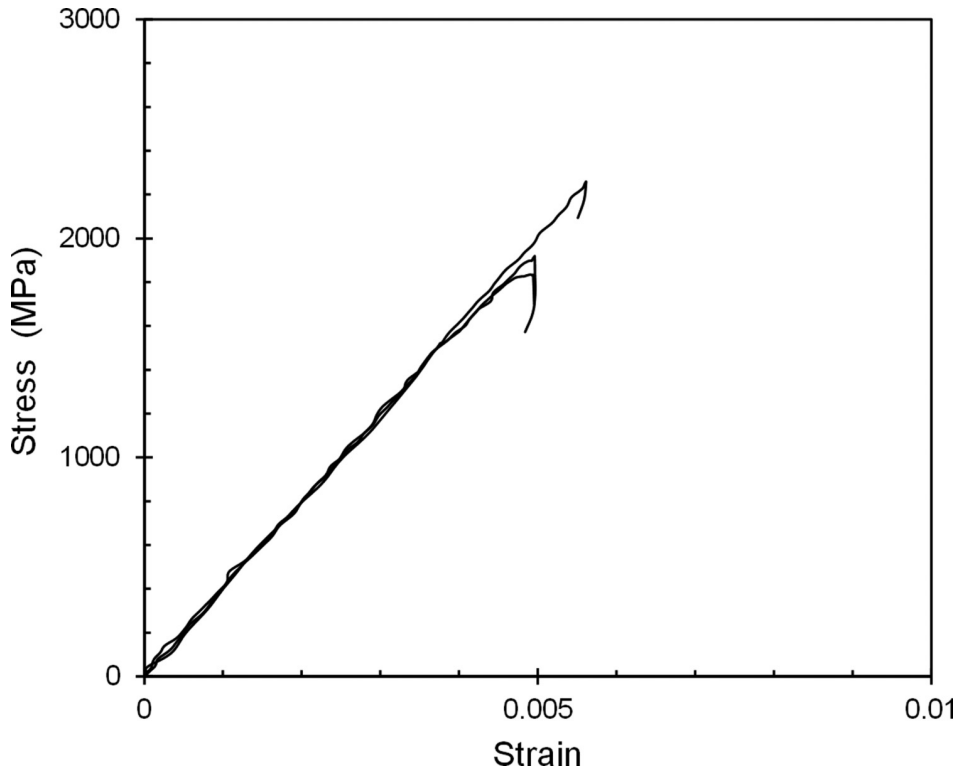

FIG. 15. Experimentally measured stress–strain curves of alumina at the quasi-static strain rate of 10^{-5} s^{-1}.

To investigate the rate dependency of alumina, compressive stress–strain response at quasi-static strain rates (10^{-5} s^{-1}) was measured in a screw-driven loading rig. As shown in Fig. 15, only elastic deformation occurs before the brittle failure at low loading rates. The failure strength increases with the loading rates (compare Figs. 14 and 15). The previous work[27] reveals that there exists a transition strain rate above which the compressive strength of ceramics increases with strain rates. In this study, the average strain rate of ~2000 s^{-1} achieved in the SHPB test may be greater than the critical rate of alumina (e.g., 100 to 400 s^{-1}).

V. CONCLUSIONS

A 3D FE model of the full scale SHPB test of alumina ceramics was developed to evaluate the stress uniformity in the specimen for the reliable characterisation of dynamic behaviour. Both the SHPB experiment and the FE simulation reveal that the forces at the specimen ends are equilibrated in the intermediate stage of deformation (i.e., approximately after five wave propagation cycles within the specimens). At the same time, the predicted stress field in the specimen becomes more uniform. The validity of stress uniformity in the specimen supports the assumption of uniaxial homogeneous deformation in the specimen and validates the SHPB test of alumina. The stress and strain histories of alumina specimens can therefore be reliably and accurately characterised in the SHPB.

ACKNOWLEDGMENTS

The authors gratefully acknowledge the financial support of the Nanyang Technological University (NTU) Start-up Grant for the research. ZW also thanks the NTU Research Student Scholarship.

[1] N. H. Murray, N. K. Bourne, and Z. Rosenberg, J. Appl. Phys. **84**, 4866 (1998).
[2] S. Sarva and S. Nemat-Nasser, Mater. Sci. Eng. A **317**, 140 (2001).
[3] J. Xu, Y. T. Sun, B. H. Liu, M. Y. Zhu, X. F. Yao, Y. Yan, Y. B. Li, and X. Chen, Eng. Fail. Anal. **18**, 1605 (2011).
[4] A. K. Mukhopadhyay, K. D. Joshi, A. Dey, R. Chakraborty, A. K. Mandal, A. Rav, J. Ghosh, S. Bysakh, S. K. Biswas, and S. C. Gupta, Ceram. Int. **37**, 2365 (2011).
[5] P. Badica, H. Borodianska, S. M. Xie, T. Zhao, D. Demirskyi, P. F. Li, A. I. Y. Tok, Y. Sakka, and O. Vasylkiv, Ceram. Int. **40**, 3053 (2014).
[6] P. Badica, S. Grasso, H. Borodianska, S. S. Xie, P. F. Li, P. Tatarko, M. J. Reece, Y. Sakka, and O. Vasylkiv, J. Ceram. Soc. Jpn. **122**, 271 (2014).
[7] L. L. Wang, J. Liang, G. D. Fang, X. Y. Wan, and J. B. Xie, Ceram. Int. **40**, 5255 (2014).
[8] S. Acharya, S. Bysakh, V. Parameswaran, and A. Kumar Mukhopadhyay, Ceram. Int. **41**, 6793 (2015).
[9] H. Sarsfield, L. Wang, and N. Petrinic, J. Mater. Sci. **42**, 5085 (2007).
[10] P. Li, C. R. Siviour, and N. Petrinic, Exp. Mech. **49**, 587 (2009).
[11] N. Gupta, D. D. Luong, and P. K. Rohatgi, J. Appl. Phys. **109**, 7 (2011).
[12] H. R. Wang, C. Y. Cai, D. N. Chen, and D. F. Ma, J. Appl. Phys. **112**, 6 (2012).
[13] R. Gerlach, C. R. Siviour, N. Petrinic, and J. Wiegand, Polymer **49**, 2728 (2008).
[14] P. Li, N. Petrinic, and C. R. Siviour, Mech. Mater. **54**, 43 (2012).
[15] Z. Wang and P. Li, Ceram. Int. **40**, 12763 (2015).
[16] G. Ravichandran and G. Subhash, J. Am. Ceram. Soc. **77**, 263 (1994).
[17] J. M. Staehler, W. W. Predebon, B. J. Pletka, and J. Lankford, J. Am. Ceram. Soc. **76**, 536 (1993).
[18] X. J. Wu and D. A. Gorham, J. Phys. IV **7**, 91 (1997).
[19] B. Song and W. Chen, Exp. Mech. **44**, 300 (2004).
[20] A. Tasdemirci and I. W. Hall, Int. J. Impact Eng. **34**, 189 (2007).
[21] J. Zhu, S. S. Hu, and L. L. Wang, Int. J. Impact Eng. **36**, 61 (2009).
[22] T. J. Holmquist and G. R. Johnson, J. Appl. Phys. **100**, 13 (2006).
[23] G. Sunny, F. Yuan, V. Prakash, and J. Lewandowski, Exp. Mech. **49**, 479 (2009).
[24] G. R. Johnson and T. J. Holmquist, AIP Conference Proceedings **309**, 981 (1994).
[25] J. M. Lifshitz and H. Leber, Int. J. Impact Eng. **15**, 723 (1994).
[26] P. Li, N. Petrinic, and C. R. Siviour, J. Appl. Phys. **110**, 083516 (2011).
[27] J. Lankford, J. Am. Ceram. Soc. **64**, C33 (1981).